applied sciences

Article

Numerical Simulation on Spatial-Frequency Domain Imaging for Estimating Optical Absorption and Scattering Properties of Two-Layered Horticultural Products

Dong Hu [1,*], Yuping Huang [2], Qiang Zhang [3], Lijian Yao [1], Zidong Yang [1] and Tong Sun [1,4,5,*]

[1] School of Engineering, Zhejiang A&F University, Hangzhou 311300, China; ljyao@zafu.edu.cn (L.Y.); 20150032@zafu.edu.cn (Z.Y.)
[2] College of Mechanical and Electronic Engineering, Nanjing Forestry University, Nanjing 210037, China; huangyuping@njfu.edu.cn
[3] Hangzhou Doubltech Electro-Hydraulic Engineering Co., Ltd., Hangzhou 310051, China; zhangqiang@deh-hydraulics.com
[4] College of Biosystems Engineering and Food Science, Zhejiang University, Hangzhou 310058, China
[5] Key Laboratory of on Site Processing Equipment for Agricultural Products, Ministry of Agriculture and Rural Affairs, Zhejiang University, Hangzhou 310058, China
* Correspondence: hudong538338@zju.edu.cn (D.H.); suntong@zafu.edu.cn (T.S.); Tel.: +86-151-5813-1053 (D.H.); +86-151-7023-0669 (T.S.)

Abstract: Spatial-frequency domain imaging (SFDI) is a wide-field, noncontact, and label-free imaging modality that is currently being explored as a new means for estimating optical absorption and scattering properties of two-layered turbid materials. The accuracy of SFDI for optical property estimation, however, depends on light transfer model and inverse algorithm. This study was therefore aimed at providing theoretical analyses of the diffusion model and inverse algorithm through numerical simulation, so as to evaluate the potential for estimating optical absorption and reduced scattering coefficients of two-layered horticultural products. The effect of varying optical properties on reflectance prediction was first simulated, which indicated that there is good separation in diffuse reflectance over a large range of spatial frequencies for different reduced scattering values in the top layer, whereas there is less separation in diffuse reflectance for different values of absorption in the top layer, and even less separation for optical properties in the bottom layer. To implement the nonlinear least-square method for extracting the optical properties of two-layered samples from Monte Carlo-generated reflectance, five curve fitting strategies with different constrained parameters were conducted and compared. The results confirmed that estimation accuracy improved as fewer variables were to be estimated each time. A stepwise method was thus suggested for estimating optical properties of two-layered samples. Four factors influencing optical property estimation of the top layer, which is the basis for accurately implementing the stepwise method, were investigated by generating absolute error contour maps. Finally, the relationship between light penetration depth and spatial frequency was studied. The results showed that penetration depth decreased with the increased spatial frequency and also optical properties, suggesting that appropriate selection of spatial frequencies for a stepwise method to estimate optical properties from two-layered samples provides potential for estimation accuracy improvement. This work lays a foundation for improving optical property estimation of two-layered horticultural products using SFDI.

Keywords: spatial-frequency domain imaging; absorption; scattering; two-layered; simulation

check for updates

Citation: Hu, D.; Huang, Y.; Zhang, Q.; Yao, L.; Yang, Z.; Sun, T. Numerical Simulation on Spatial-Frequency Domain Imaging for Estimating Optical Absorption and Scattering Properties of Two-Layered Horticultural Products. *Appl. Sci.* **2021**, *11*, 617. https://doi.org/10.3390/app11020617

Received: 9 December 2020
Accepted: 7 January 2021
Published: 10 January 2021

1. Introduction

Optical absorption (μ_a) and reduced scattering coefficients ($\mu_s{}'$) are closely related to tissue physicochemical properties (e.g., tissue porosity, particle size distribution, etc.), which, in turn, could be used as a means for enhancing the nondestructive quality and safety evaluation (e.g., firmness, soluble solids content, titratable acidity, etc.) of horticultural products. In the last two decades, measuring optical properties (i.e., μ_a and $\mu_s{}'$) of horticultural products (e.g., apple, citrus and tomato) have been widely studied by different researchers in the field of food and agricultural engineering [1–3]. It was reported that the multiplication of absorption and reduced scattering coefficients of tomato tissues measured by spatially-resolved techniques were highly correlated with flesh firmness, with a correlation coefficient of 0.835 [1]. In the study of Vanoli et al. (2020) [3], absorption and reduced scattering coefficients of 'Braeburn' apples were determined, which were used to evaluate the ripening processes during the shelf life period, as absorption phenomena were related to changes in pigments present in the fruit flesh and peel, while scattering events mirrored changes in the flesh texture.

Most research teams treated the samples as homogeneous media and neglected the difference of optical properties among different layers for simplifying parameter estimation procedure. However, this simplification could bring errors in studying the optical properties, as well as the loss of critical physicochemical information for individual layers. Efforts have been made on developing two- and multi-layered models for measuring μ_a and $\mu_s{}'$ of each layer in the traverse direction (i.e., along the surface of a turbid sample) [4–7], but the estimation errors reported in most studies are still too large and unacceptable, especially for the second or bottom layer. For example, Cen and Lu (2009) estimated the optical properties of two-layered turbid materials simultaneously by using spatially-resolved techniques [5]. The results showed that absorption and reduced scattering coefficients of the top layer of the model samples were determined with errors within 23.0 and 18.4%, respectively, while the inverse algorithm did not give acceptable estimations for the bottom layer. Weber et al. (2009) applied the technique of spatial-frequency domain imaging (SFDI) to estimate optical properties of layered tissues, and reported average accuracies of ±2 and ±17% for absorption and reduced scattering coefficients of the top layer, respectively, by using the four-parameter fit [8]. However, the estimation errors for absorption coefficients of the bottom layer were as large as ±25%, and no acceptable estimations for the bottom-layer's reduced scattering coefficients, even with the two-parameter fit. The major reason causing the large estimation error is the much more complex inverse algorithm for a two-layered model since it has five optical parameters (i.e., μ_a and $\mu_s{}'$ of each layer, plus the unknown thickness of the top layer). It is, therefore, desirable to understand the intrinsic properties of the two-layered model prior to implementing an inverse algorithm for optical property estimation. Cen and Lu (2009) conducted sensitivity analysis to study the effects of optical parameters (μ_{a1}, $\mu_{s1}{}'$, μ_{a2}, $\mu_{s2}{}'$ and R_d, where subscripts 1 and 2 refer to the top and bottom layer, and R_d is diffuse reflectance) in a two-layered model on optical property estimation by using spatially-resolved technique [5], while Wang et al. (2019) studied the effects of five optical parameters (μ_{a1}, $\mu_{s1}{}'$, μ_{a2}, $\mu_{s2}{}'$ and top-layer thickness d) on reflectance prediction with the technique of spatially-resolved [7]. However, few studies were focused on the theoretical analysis of intrinsic properties of two-layered diffusion model in SFDI for optical property estimations.

As an emerging optical measuring technique, SFDI is capable of noncontact and wide-field mapping of μ_a and $\mu_s{}'$ on a pixel-by-pixel basis, which is absent in other techniques using point light source (e.g., spatially-resolved, time-resolved, and integrating sphere). SFDI can be used for estimating optical properties of homogeneous tissues, as well as layered samples, by using appropriate light transfer models (e.g., diffusion approximation and Monte Carlo). Recently, Tabassum et al. (2018) developed a two-layer look-up-table inversion algorithm for extracting μ_a and $\mu_s{}'$of the bottom layer, in which Monte Carlo simulations were conducted natively in the spatial-frequency domain [9]. The results showed that optical property extractions of the bottom (tumor) layer were determined to be within 20 and 11% of the true values for μ_a and $\mu_s{}'$, respectively. Several other studies have also been reported for estimating μ_a and $\mu_s{}'$ of layered tissues using the SFDI technique [8–12]. Some researchers estimated the four optical properties (μ_{a1}, $\mu_{s1}{}'$, μ_{a2} and $\mu_{s2}{}'$) simultaneously with the known top-layer thickness (all-at-once method) [8], while others estimated μ_a and $\mu_s{}'$ of one (often the top) layer first, followed by estimating μ_a and $\mu_s{}'$ of the other layer (stepwise method) [12]. Our previous study demonstrated that the efficacy and accuracy of the stepwise method for estimating optical properties of two-layered samples were superior to that for the all-at-once method, under the constraining conditions for the top-layer thickness between 0.2 and 2.0 mm [13]. In the paper of our recent research, the stepwise method with frequency optimization was employed for measuring the optical properties of apple peel and flesh tissues, and the results showed that there were still relatively large error values (22.8%) for estimating absorption coefficient of the flesh tissue due to the theoretical difficulty in estimating absorption coefficient of the bottom layer [12].

In the stepwise method, accurate measurement of the optical properties of the top layer is critical, because optical property estimations of the bottom layer is based on those of the top layer (i.e., the estimated μ_{a1} and $\mu_{s1}{}'$ are treated as known variables for estimating μ_{a2} and $\mu_{s2}{}'$ with the two-layered diffusion model). Therefore, effects of potential influencing factors, such as relative values of the optical properties of two layers ($mfp_1{}'/mfp_2{}'$, μ_{a1}/μ_{a2} and $\mu_{s1}{}'/\mu_{s2}{}'$) and relative values of $\mu_{s1}{}'$ and μ_{a1} ($\mu_{s1}{}'/\mu_{a1}$) on optical property extraction of the top layer, should be quantitatively described and considered. It should be noted that mfp' [$= 1/(\mu_a + \mu_s{}')$] is short for mean free path, which denotes the mean distance of a single step as an energy packet travels within the tissues. Moreover, accurate optical property estimation of two-layered horticultural products with SFDI relies on selecting appropriate curve fitting method, which may have diverse types in terms of free variables. For the two-layered diffusion model that has five unknown variables, the free variable(s) can range from one to five, in principle, depending on the number of constrained parameters. It is expected that evaluation of estimation accuracy of different curve fitting methods would verify that the stepwise method proposed in our previous study has better accuracy than all other curve fitting strategies for estimating optical properties of two-layered samples. In addition, it is preferable to have low light penetration depth when estimating optical properties of the top layer, while high penetration depth is welcome for the bottom layer, due to the fact that detected light should carry more effective information with the target layer. It is reported that light penetration depth in SFDI is closely related to spatial frequency [14]. Hence, it is desirable to quantitatively investigate the relationship between light penetration depth and spatial frequency, in order to improve the optical property estimation of two-layered horticultural products.

This paper presents a theoretical analysis of intrinsic properties of two-layered diffusion model and inverse algorithm through numerical simulation in order to improve optical property estimation using the SFDI technique. Therefore, the objectives of this research were to: (1) explore the effect of optical parameters (μ_{a1}, $\mu_{s1}{}'$, μ_{a2} and $\mu_{s2}{}'$) on reflectance prediction; (2) evaluate parameter estimation accuracy of different curve fitting methods for optical property estimations of two-layered samples; (3) investigate potential influencing factors on optical property estimations of the top layer for accurately implementing the stepwise method; (4) study the relationship between light penetration depth and spatial frequency for laying a foundation for frequency optimization.

2. Materials and Methods

2.1. Principle and Diffusion Model

Previous literature has described the principles of SFDI for optical property estimation of turbid media based on diffusion model [13,15], so only a brief description will be provided here. Although not accurate for all optical properties, the diffusion model, which is a simplified form of the radiative transfer equation, remains an efficient tool to model light propagation in turbid media by providing analytical solutions that are easily implemented and intuitive. For a homogeneous one-layered medium of semi-infinite geometry normally illuminated at its surface by a steady-state, planar sinusoidal light pattern, diffuse reflectance at the surface can be yielded by applying the partial-current boundary condition [16]:

$$R_d(f_x) = \frac{3Aa'}{\left(\mu'_{eff}/\mu_{tr} + 1\right)\left(\mu'_{eff}/\mu_{tr} + 3A\right)} \tag{1}$$

where $A = \frac{1-R_{eff}}{2(1+R_{eff})}$ is proportionality constant, $R_{eff} \approx 0.0636n + 0.668 + 0.71/n - 1.44/n^2$ is the effective reflection coefficient, in which n is the refractive index of the medium, $a' = \mu'_s/\mu_{tr}$ is the reduced albedo, $\mu_{tr} = \mu_a + \mu'_s$ is the transport coefficient, μ_a and $\mu_s{}'$ are absorption coefficient and reduced scattering coefficient, respectively, $\mu'_{eff} = \left(3\mu_a\mu_{tr} + (2\pi f_x)^2\right)^{1/2}$ is the scalar attenuation coefficient, and f_x is the spatial frequency.

For a two-layered turbid medium (Figure 1), light within the medium decays exponentially, such that the light source term is different in each layer with the bottom layer being assumed to be infinitely thick. By applying appropriate boundary conditions to the diffusion model, diffuse reflectance at the surface can be expressed using Equation (2) [17]:

$$R_d(f_x) = A \cdot \frac{\mu'_{s1}}{\mu'_{eff1}} \cdot \frac{A_1 + A_2}{A_3} x \tag{2}$$

where A_1, A_2 and A_3 are constants determined by the boundary conditions, and subscript 1 of $\mu_{s1}{}'$ and $\mu_{eff1}{}'$ refers to the top layer.

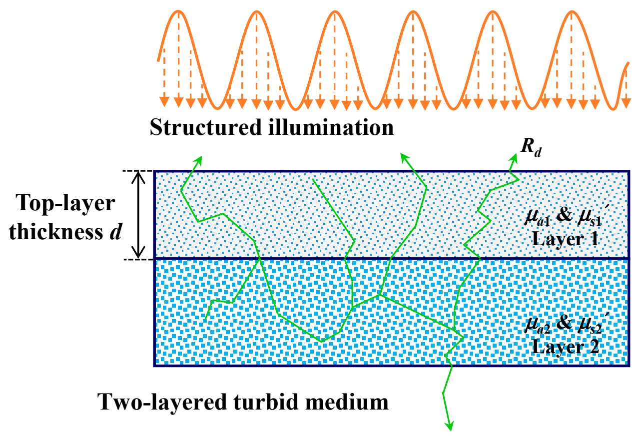

Figure 1. Schematic of a two-layered turbid medium under structured illumination. μ_{a1}, μ_{a2}, $\mu_{s1}{}'$ and $\mu_{s2}{}'$ are absorption and reduced scattering coefficients for the top layer and bottom layer, respectively, d is the thickness of the top layer, and R_d is the diffuse reflectance at the surface.

2.2. Monte Carlo Simulations

Monte Carlo (MC) offers a flexible and accurate approach for modeling light propagation within tissues [18]. In order to investigate the effects of different optical properties on reflectance prediction from the two-layered diffusion model, to evaluate the estimation accuracy of different curve fitting methods, and to analyze the factors influencing optical property extraction of the top layer, a publicly available MC simulation program for multi-layered turbid media was used [19]. In the simulations, a package of five million photons was tracked. The maximum radial distance of the medium was set to 50 mm, which is large enough to be treated as semi-infinite. The spatial resolution for both radial distance and depth was set to 0.1 mm. The average refractive indices of the two-layered media were both chosen to be 1.35, which was typical for most horticultural products (e.g., apple, blueberry, citrus, tomato etc.) [20,21], while the media above and beneath the tissue were treated as air, with the refractive index of 1.0. The anisotropy factor g was set to 0.9, and Henyey–Greenstein phase function was used to describe light scattering.

More details about the phase function can be found in reference by Henyey and Greenstein (1941) [22]. The Monte Carlo multi-layered (MCML) program was first applied to generate the spatially-resolved diffuse reflectance profiles of two-layered samples along the radial distance under the normal incidence of an infinite small light source. Then the 1-D Hankel transform of order zero was used to convert the spatially-resolved reflectance to spatial-frequency domain reflectance [16], which was further used for evaluating the curve fitting methods and investigating the potential influencing factors through optical property estimations.

In this study, a total of 20 combinations of μ_a and $\mu_s{}'$ for two-layered samples (five samples with varying μ_a or $\mu_s{}'$ of each layer with the top-layer thickness of 2 mm, Table S1 in Supplementary Materials) were prepared for investigating the effects of optical properties on reflectance prediction and comparing the estimation accuracy of diverse curve fitting methods. One optical property value was varied, while the other four were held constant. The optical property values for these samples were chosen based on published data [23–25], covering a large range of horticultural products with 0.001 mm^{-1} $\leq \mu_a \leq$ 0.1 mm^{-1} and 0.5 mm^{-1} $\leq \mu_s{}' \leq$ 4 mm^{-1}. More simulation samples were created (see Tables S2–S5 in Supplementary Materials for more details) for studying the effects of relative values of the optical properties of two layers ($mfp_1{}'/mfp_2{}'$, μ_{a1}/μ_{a2} and $\mu_{s1}{}'/\mu_{s2}{}'$) and relative values of $\mu_{s1}{}'$and μ_{a1} ($\mu_{s1}{}'/\mu_{a1}$), for optical property extraction from the top layer. The parameters of μ_{a1}/μ_{a2} and $\mu_{s1}{}'/\mu_{s2}{}'$ were selected for studying the contributions of absorption and reduced scattering coefficients of two layers on estimating optical properties of the top layer, respectively, while $mfp_1{}'/mfp_2{}'$ was used for studying the combination effect of absorption and reduced scattering coefficients. The diffusion model is based on the assumption that scattering is dominant over absorption ($\mu_s{}' >> \mu_a$), so the parameter of $\mu_{s1}{}'/\mu_{a1}$ was also selected for investigating its effect on optical property estimation. Hereinafter, these relative values are called influencing factors for convenience. Our previous study has investigated the effect of top-layer thickness on optical property estimation of two-layered medium and also determined the constraining conditions [13], indicating that the top-layer's maximum thickness could not exceed 2 mm, in order to have acceptable estimations of optical properties of the bottom layer. Hence the top-layer thickness was chosen to be 2 mm for all the simulation samples in this study.

2.3. Inverse Algorithm for Estimating Optical Properties of Two-Layered Samples

Prior to determining the optical properties of two-layered simulation samples from the spatial-frequency domain reflectance, the effect of varied μ_a and $\mu_s{}'$ of each layer on reflectance prediction was investigated, which would be helpful for understanding the two-layered diffusion model. To select the most proper, robust and accurate parameter estimation method for determining the optical properties of two-layered samples, different curve fitting methods that differ in the number of free variables were compared and evaluated (Table 1). First, all five parameters (μ_{a1}, $\mu_{s1}{}'$, μ_{a2}, $\mu_{s2}{}'$ and d) were estimated simultaneously using the two-layered model in Equation (2) (five-variable fit). Second, the top-layer thickness was assumed to be known and the other four parameters were estimated at once (four-variable fit). Third, μ_a and $\mu_s{}'$ of either the top layer or the bottom layer were estimated, depending on which layer had changed variables, while μ_a and $\mu_s{}'$ of the other layer and thickness the top layer were treated as known (two-variable fit). Fourth, only μ_a or $\mu_s{}'$ was estimated, while all others were treated as known (one-variable fit). Fifth and finally, the one-layered model in Equation (1) was utilized to estimate μ_a and $\mu_s{}'$ of the top layer, which was used in our proposed stepwise method [13]. The estimated optical properties were compared with the true values for evaluating the estimation accuracy.

Table 1. Different curve fitting methods for estimating optical properties of two-layered simulation samples.

Curve Fitting Method	Estimated Parameter	Known Parameter	Fitted Model
Five-variable fit	μ_{a1}, μ_{s1}', μ_{a2}, μ_{s2}', d	–	Equation (2)
Four-variable fit	μ_{a1}, μ_{s1}', μ_{a2}, μ_{s2}'	d	Equation (2)
Two-variable fit	μ_{a1}, μ_{s1}' or μ_{a2}, μ_{s2}',	the other three	Equation (2)
One-variable fit	μ_{a1} or μ_{s1}' or μ_{a2} or μ_{s2}'	the other four	Equation (2)
One-layered model	μ_{a1}, μ_{s1}'	–	Equation (1)

A nonlinear least-squares fitting method was used to minimize the sum-of-squares of the difference between the true reflectance and predicted reflectance values with estimated parameters using Equation (1) or Equation (2). In this study, a subspace trust-region method based on the interior-reflective Newton approach was used to achieve the algorithm optimization [26], which is defined by minimizing a quadratic function subject to an ellipsoidal constraint. The approach can generate iterates in the strictly feasible region by using a new affine scaling transformation, and the speed of convergence is accelerated by following a reflective line search technique. The optical property estimation procedure from the spatial-frequency domain reflectance of two-layered simulation samples was implemented using the Toolbox function 'lsqcurvefit' in Matlab 8.4 (The MathWorks, Inc., Natick, MA, USA). Previous studies revealed that there were inherent discrepancies of the reflectance between the diffusion model and MC simulation, which would greatly affect the accuracy of optical property estimation [16,27]. It was proven that sample-based calibration method could decrease the reflectance discrepancies and improve the estimation accuracy. The method was implemented by first selecting a set of calibration samples depending on the initial estimated values of μ_{s1}'. Ratios of diffusion model generated reflectance to MC-generated reflectance for all the calibration samples were obtained, and they were then used for calculating the calibrated reflectance by multiplying the original reflectance for each sample. Since this study is focused on theoretical analysis of a two-layered diffusion model, the sample-based calibration method was thus applied for reflectance correction, which was then used for optical property estimation. More details about the calibration method are referred to Hu et al. (2019) [13].

To qualitatively and quantitatively investigate the factors influencing optical property estimation of the top layer, absolute error contour maps for estimating μ_a and μ_s' were plotted, with the horizontal and vertical axes of the maps denoting start and end spatial frequencies, in which the error was calculated by comparing the true values of μ_a and μ_s' with the parameter estimation results. Eleven start frequencies from 0 to $0.1/mfp_1'$ with an increment of $0.01/mfp_1'$ and 18 end frequencies from $0.15/mfp_1'$ to $0.5/mfp_1'$ with an increment of $0.02/mfp_1'$ were evaluated for parameter estimations of the top layer. The interval spacing between each start and end frequency pair was set as 0.01 mm^{-1}. Note that relative errors in contour maps were transformed to absolute values, and the absolute errors of μ_a and μ_s' larger than 60% and 20% were treated as 60% and 20% for better visual effect.

3. Results

3.1. Effect of Varying Optical Properties on Diffuse Reflectance

Frequency-dependent diffuse reflectance predicted by the two-layered diffusion model for different optical properties of each layer is plotted in Figure 2; for each plot in the figure one parameter is varied while the other four are held constant. Generally, the reflectance decreased with the increased absorption coefficients, while it increased with the reduced scattering coefficients. The most distinct separation in diffuse reflectance for different values of μ_{a1}, μ_{a2} and μ_{s2}' was observed at relatively low frequencies. For varying μ_{s1}' values, the five reflectance curves show distinct differences across the frequency range with the best separation occurring around 0.2 mm^{-1} (Figure 2(a2)). Overall, Figure 2 demonstrates that there is good separation in diffuse reflectance over a large range of spatial frequencies for different μ_{s1}' values, whereas less separation in diffuse reflectance for different μ_{a1} values, and even less separation for different values of μ_{a2} and μ_{s2}', suggesting the difficulty of accurately estimating the bottom layer. That is because light must propagate through the top layer before interacting with the bottom layer tissue, in which case only a small number of energy packets reemitted from the bottom layer can be detected. In Figure 2(b1,b2), the value of mfp_1' is equal to 0.5 mm, while the top-layer thickness is 2 mm, which implies that light would have travelled more than four steps before entering into the bottom layer. Hence, the separation in diffuse reflectance for different values of μ_{a2} and μ_{s2}' would increase with the decreased top-layer thickness due to the fact that the detected light have more interaction with the bottom layer. The results from the four plots in Figure 2 further suggest that better estimation of the four optical parameters (μ_{a1}, μ_{s1}', μ_{a2} and μ_{s2}') could be achieved when low spatial frequencies are used.

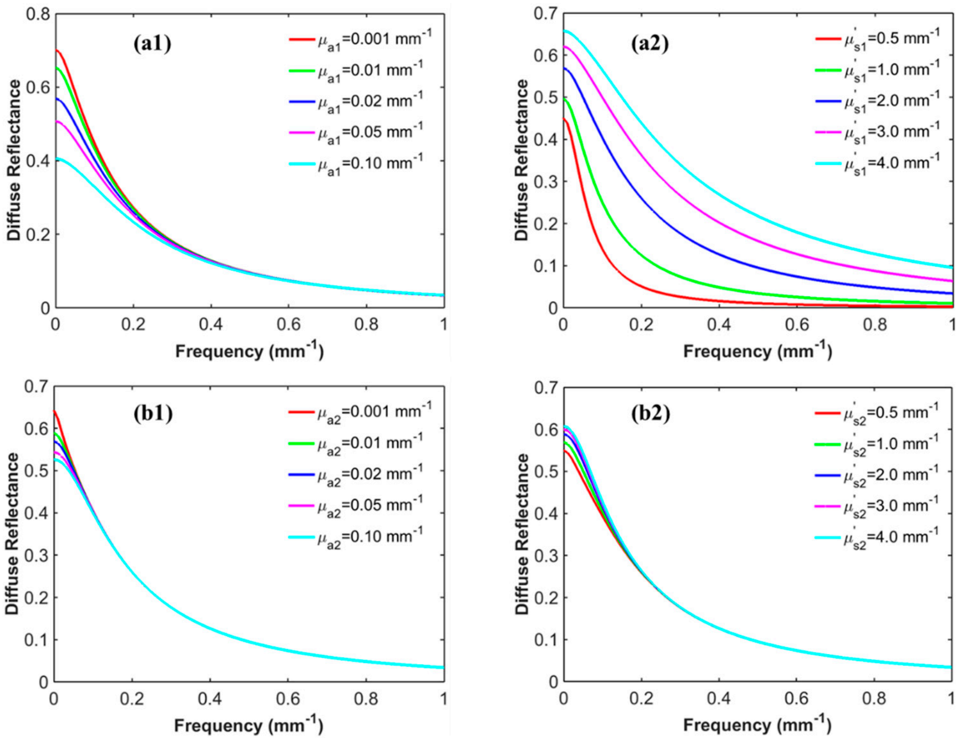

Figure 2. Diffuse reflectance predicted by the two-layered diffusion model (Equation (2)) versus spatial frequency for varying optical properties in (**a1**) μ_{a1} (μ_{s1}' = 2 mm^{-1}, μ_{a2} = 0.02 mm^{-1}, μ_{s2}' = 1 mm^{-1} and d = 2 mm), (**a2**) μ_{s1}' (μ_{a1} = 0.03 mm^{-1}, μ_{a2} = 0.02 mm^{-1}, μ_{s2}' = 1 mm^{-1} and d = 2 mm), (**b1**) μ_{a2} (μ_{a1} = 0.03 mm^{-1}, μ_{s1}' = 2 mm^{-1}, μ_{s2}' = 1 mm^{-1} and d = 2 mm), and (**b2**) μ_{s2}' (μ_{a1} = 0.03 mm^{-1}, μ_{s1}' = 2 mm^{-1}, μ_{a2} = 0.02 mm^{-1} and d = 2 mm).

3.2. Optical Property Extraction from MC-Generated Reflectance

As mentioned in Section 2.3, the reflectance generated by MC simulation, after the correction, was much closer to that by the diffusion model, which was, therefore, used for optical property extraction in this study. Figure 3 shows estimated absorption and reduced scattering coefficients of each layer using different curve fitting methods. Note that the one-layered model was only used for estimating μ_{a1} and μ_{s1}' in Figure 3(a1,a2). The average absolute values of relative errors for the five curve fitting methods are summarized in Table 2. Overall, the accuracy for estimating μ_{a1}, μ_{s1}', μ_{a2} and μ_{s2}' from the corrected reflectance are within 18%, which are superior to that without reflectance correction (results not presented here).

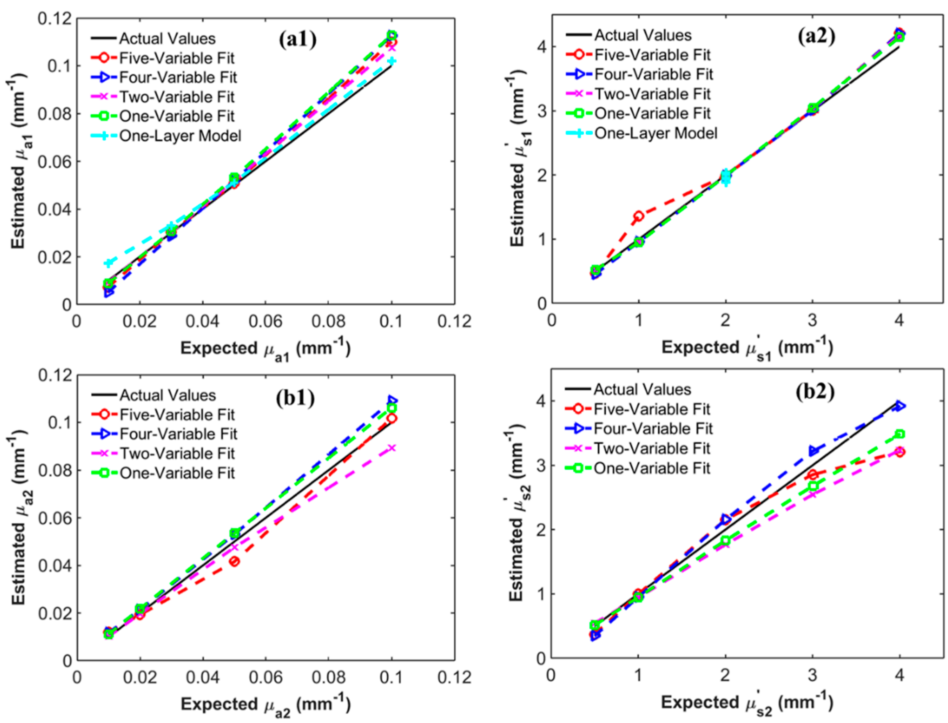

Figure 3. Estimated absorption and reduced scattering coefficients of each layer from the corrected reflectance generated by Monte Carlo simulation using different curve fitting methods. (**a1**) μ_{a1} varies 0.01–0.1 mm^{-1} with μ_{s1}' = 2 mm^{-1}, μ_{a2} = 0.02 mm^{-1}, μ_{s2}' = 1 mm^{-1} and d = 2 mm, (**a2**) μ_{s1}' varies 0.5–4 mm^{-1} with μ_{a1} = 0.03 mm^{-1}, μ_{a2} = 0.02 mm^{-1}, μ_{s2}' = 1 mm^{-1} and d = 2 mm, (**b1**) μ_{a2} varies 0.01–0.1 mm^{-1} with μ_{a1} = 0.03 mm^{-1}, μ_{s1}' = 2 mm^{-1}, μ_{s2}' = 1 mm^{-1} and d = 2 mm, and (**b2**) μ_{s2}' varies 0.5–4 mm^{-1} with μ_{a1} = 0.03 mm^{-1}, μ_{s1}' = 2 mm^{-1}, μ_{a2} = 0.02 mm^{-1} and d = 2 mm.

Table 2. Average relative errors (in absolute values) of different curve fitting methods for estimating absorption (μ_a) and reduced scattering (μ_s') coefficients of each layer.

Optical Property	Five-Variable Fit	Four-Variable Fit	Two-Variable Fit	One-Variable Fit	One-Layered Model
μ_{a1} (%)	9.84	17.25	4.78	8.14	12.23
μ_{s1}' (%)	9.81	3.72	2.77	2.90	2.66
μ_{a2} (%)	10.44	9.86	4.73	8.30	–
μ_{s2}' (%)	11.62	10.48	12.11	8.15	–

The accuracy for estimating μ_{s1}' (Figure 3(a2)) was much better than that for μ_{a1} (Figure 3(a1)) for all five curve fitting methods, which is consistent with the reflectance analyses in Section 3.1. It could be observed from Table 2 that five-variable fit performed the weakest for estimating μ_{s1}', followed by the four-variable fit, confirming that estimation accuracy improves as fewer variables are to be estimated each time [5,7]. However, for estimating μ_{a1}, four-variable fit performed the weakest, followed by the one-layered model. These results are out of expectation that one-layered model with two unknown variables could obtain higher estimation accuracy than five- and four-variable fit methods. This may be partly explained by the fact that the light samples the bottom layer as well thus seeing in part its increased absorption, especially for lower μ_{a1}, while for high μ_{a1}, the detected light does no longer go through the bottom layer, making the one-layered model a well description. Moreover, the reflectance used for curve fitting was generated by MC simulation and corrected based on the values of μ_{s1}' rather than μ_{a1}, which may also add challenges for estimating μ_{a1} using the one-layered model; the value of μ_{a1} is much smaller and more sensitive to the reflectance change than the μ_{s1}'. Detailed analyses show that the largest average error for estimating μ_{a1} using one-layered model is caused by the first point where μ_{a1} is equal to 0.01 mm^{-1} (shown in Figure 3(a1)).

For the bottom layer estimation in Figure 3(b1,b2)), estimation accuracy is much worse than for the top layer. Two- and one-variable fit improved the accuracy for estimating μ_{a1}, $\mu_{s1}{}'$ and μ_{a2}, but the error values for estimating $\mu_{s2}{}'$ using the two-variable fit were a little higher than the other three methods (Table 2). It is expected that the estimation accuracy of μ_{a2} and $\mu_{s2}{}'$ would be improved as the top-layer thickness decreases, because the detected light would carry more information related to the bottom layer.

In view of the fact that no a priori information about the optical properties of the bottom layer is available in practical applications, and after comparison of the average absolute errors for all five curve fitting methods, a stepwise method is suggested for estimating the optical properties of two-layered samples. First, μ_{a1} and $\mu_{s1}{}'$ are estimated using one-layered model. After obtaining μ_{a1} and $\mu_{s1}{}'$ estimations, the two-variable fit is used for estimating μ_{a2} and $\mu_{s2}{}'$, assuming that the top-layer thickness is known. It should be noted that one-layered model does not require a priori knowledge of the top-layer thickness for estimating μ_{a1} and $\mu_{s1}{}'$, compared to the other curve fitting methods (i.e., four-, two- and one-variable fit). The stepwise method reduces the number of constrained variables from five or four to two at every step, which could improve the overall estimation accuracy [12,13]. Therefore, the stepwise method was used for optical property estimations of two-layered samples going forward after Section 3.2 in this study.

3.3. Factors Influencing Optical Property Extraction of Top Layer

Accurate optical property extraction from the top layer is critical for the stepwise method because estimation results of the bottom layer are based on those from the top layer. Influencing factors of $mfp_1{}'/mfp_2{}'$, μ_{a1}/μ_{a2} and $\mu_{s1}{}'/\mu_{s2}{}'$ determine the contributions of each layer on diffuse reflectance. Larger contribution implies higher accuracy for estimating the corresponding optical properties theoretically. Parameter of $\mu_{s1}{}'/\mu_{a1}$ is closely related to the assumption of diffusion model, which is the basis of Equation (1) and Equation (2) for optical property estimation. It is thus desirable to quantitatively evaluate the effects of the four factors. The results showed that factors of μ_{a1}/μ_{a2} and $\mu_{s1}{}'/\mu_{s2}{}'$ had negligible effects on optical property extraction from the top layer (see Figures S1 and S2 in Supplementary Materials for more details). Hence only the factors of $mfp_1{}'/mfp_2{}'$ and $\mu_{s1}{}'/\mu_{a1}$ are discussed here, and the results are displayed in Figures 4 and 5, respectively.

It is observed from Figure 4 that the absolute values of relative errors for estimating μ_{a1} and $\mu_{s1}{}'$ decreased first, and then increased with the increasing values of $mfp_1{}'/mfp_2{}'$. Further analysis showed that there were relatively small errors for μ_{a1} and $\mu_{s1}{}'$ when the values of $mfp_1{}'/mfp_2{}'$ were 1.2 and 1.6 (No. 26 and No. 27 in Table S2 of Supplementary Materials). This may be due to that the effective attenuation coefficients μ_{eff} of the bottom layer (1.36 and 1.57) and the top layer (1.60 and 1.60) are close to each other for both the two samples, resulting in similar light attenuation for the two layers. The absolute error contour maps also indicated that the optimal frequency region for estimating $\mu_{s1}{}'$ was rather stable with relatively large start and end frequencies. This is because diffuse reflectance under large spatial frequency mainly depends on tissue scattering properties. For μ_{a1}, it is observed that the optimal start and end frequencies increased when the values of $mfp_1{}'/mfp_2{}'$ raised from 0.4 to 1.2 (Figure 4(a1,b1,c1)) due to the fact that larger $mfp_1{}'/mfp_2{}'$ lead to increased optical properties for the bottom layer, resulting in more effects on optical property estimations of the top layer. It was reported that structured illumination with larger frequencies resulted in shallower light interrogation [14,16,28], thus reducing and even eliminating the effects of the bottom layer on the estimation of μ_{a1} and $\mu_{s1}{}'$. These findings could provide references for optimizing frequency region for optical property estimations from the spatial-frequency domain reflectance.

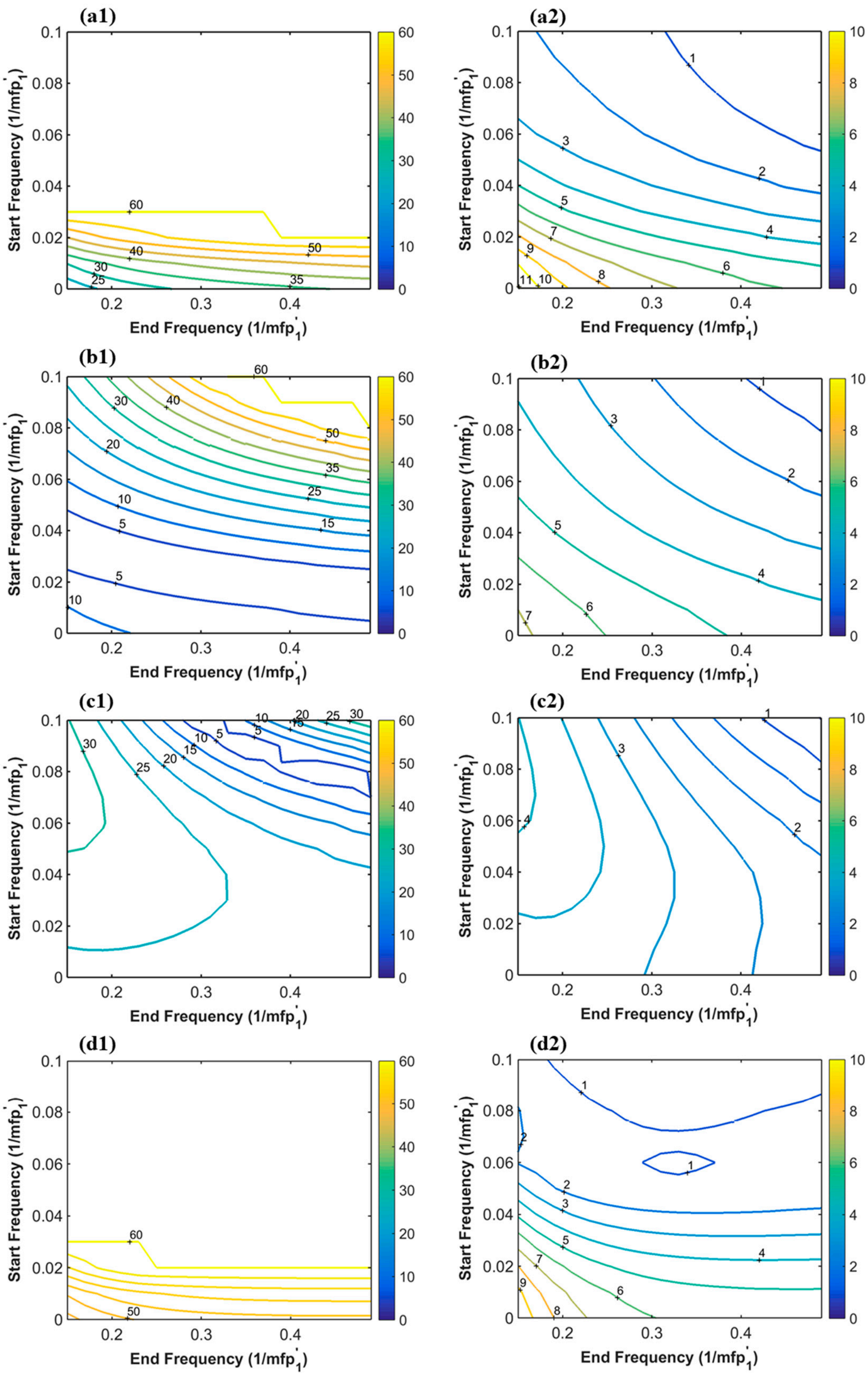

Figure 4. Absolute error contour maps for estimating μ_{a1} (**left panel**) and μ_{s1}' (**right panel**) of four representative two-layered simulation samples with varying values of mfp_1'/mfp_2' by using the stepwise method with different start and end frequencies. The values of mfp_1'/mfp_2' were 0.4, 0.8, 1.2 and 4 for (**a**), (**b**), (**c**) and (**d**), respectively. Different colors in the vertical bars on right of each graph denote different levels of error in percentage. Note that the absolute errors of μ_{a1} and μ_{s1}' larger than 60 and 20% were treated as 60 and 20% for better visual effect.

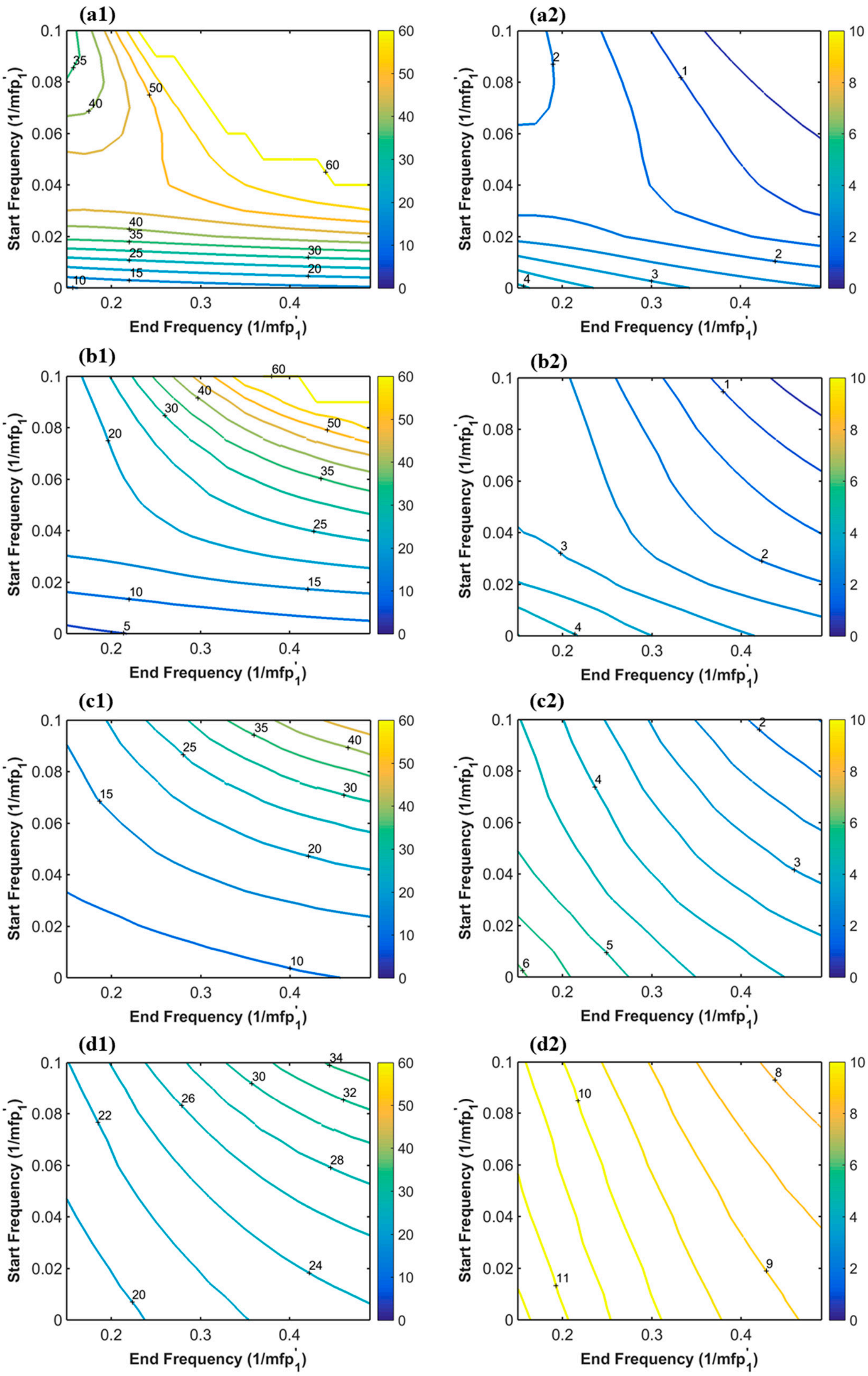

Figure 5. Absolute error contour maps for estimating μ_{a1} (**left panel**) and $\mu_{s1}{}'$ (**right panel**) of four representative two-layered simulation samples with varying values of $\mu_{s1}{}'/\mu_{a1}$ by using the stepwise method with different start and end frequencies. The values of $\mu_{s1}{}'/\mu_{a1}$ were 133, 50, 20 and 5 for (**a**), (**b**), (**c**) and (**d**), respectively. Different colors in the vertical bars on right of each graph denote different levels of error in percentage. Note that the absolute errors of μ_{a1} and $\mu_{s1}{}'$ larger than 60 and 20% were treated as 60 and 20% for better visual effect.

Figure 5 showed that the optimal frequency region for estimating both μ_{a1} and μ_{s1}' were relatively stable with varying values of μ_{s1}'/μ_{a1}. Absolute values of relative errors for estimating μ_{s1}' increased with the decreased values of μ_{s1}'/μ_{a1}, which is in agreement with the expectation since the curve fitting is subject to the assumption of diffusion approximation (i.e., scattering dominant tissue). However, the error pattern for estimating μ_{a1} did not obey this strictly. The absolute values of relative errors of μ_{a1} reduced with the values of μ_{s1}'/μ_{a1} decreasing from 133 to 20. Further analysis demonstrated that smaller μ_{s1}'/μ_{a1} lead to larger values of μ_{a1}, which made μ_{a1} be less sensitive to the variation and the parameter estimation for μ_{a1} much easier (e.g., errors could reduce from 10 to 1% for μ_{a1} values of 0.01 mm^{-1} and 0.1 mm^{-1}, respectively, when the measured value deviated 0.001 mm^{-1} from the true value); even so, errors for estimating μ_{a1} increased when the values of μ_{s1}'/μ_{a1} were smaller than 10 (Figure 5(d1)), because too small μ_{s1}'/μ_{a1} was beyond the boundary in which the optical properties could be estimated accurately from the diffusion model.

Overall, the discussion above suggests that the values of μ_{s1}'/μ_{a1} should be no smaller than 10 to obtain accurate estimation of μ_{a1} and μ_{s1}' by using the stepwise method, which is applicable for most horticultural products due to the scattering-dominated property. Considering the findings that the optimal frequency region for estimating μ_{a1} (that for μ_{s1}' is relatively stable) varies with the values of mfp_1'/mfp_2', it is strongly suggested to optimize the spatial frequency in terms of mfp_1' and/or mfp_2' for improving the estimation accuracy in future studies.

3.4. Relationship Between Light Penetration Depth and Spatial Frequency

Knowledge of light penetration depth is valuable because it could help us in optimizing the design of sensing configuration and parameter (i.e., illumination/detection geometry, sample presentation mode, detection angle, etc.) to collect effective information from the interior tissue of a target sample. Different methods have been proposed for measuring light penetration depth [29–33]. In diffuse optics, light penetration depth in horticultural products is typically defined as the travelling distance corresponding to a decay in power by a factor of $1/e$ (~37%). In the context of the steady-state diffuse approximation, light penetration depth of conventional uniform illumination depends on tissue optical properties (i.e., μ_a and μ_s'), which can be calculated using the following equation [34]:

$$\delta = \frac{1}{\mu_{eff}} = \frac{1}{\sqrt{3\mu_a\left(\mu_a + \mu_s'\right)}} \tag{3}$$

where μ_{eff} is the effective attenuation coefficient. Under structured illumination of sinusoidal patterns in SFDI technique, the above equation can be modified as follows [16,35]:

$$\delta = \frac{1}{\mu_{eff}'} = \frac{1}{\sqrt{\mu_{eff}^2 + \left(2\pi f_x\right)^2 + \left(2\pi f_y\right)^2}} \tag{4}$$

where f_x and f_y are spatial frequencies along horizontal and vertical directions, respectively.

Equation (4) implies that light penetration depth under structured illumination depends, besides the tissue optical properties, on the spatial frequency of the sinusoidal patterns. High spatial frequency results in shallow penetration depth, which provides a theoretical guide for achieving the effective information in different depths by selecting appropriate spatial frequencies. Four sets of optical properties, which cover the common and typical range of horticultural products, were employed for studying the relationship between light penetration depth and spatial frequency, and the results are displayed in Figure 6. It could be observed that larger values of μ_a and μ_s' generated shallower light penetration depth (pink dot line) since more light was absorbed or scattered while propagating within the tissues. This trend is especially true when the spatial frequency is smaller than 0.05 mm^{-1}. According to this, the light penetration depth is estimated to be 0.5–5.5 mm for apple fruit with typical values of μ_a being 0.01–0.05 mm^{-1} and $\mu_s{}'$ being 1.0–2.0 mm^{-1}, respectively, in the wavelength region of 500–1000 nm. Note that the illumination pattern in this case is modulated only along the horizontal axis (i.e., f_y = 0) with the spatial frequency f_x varying from 0.01 to 0.3 mm^{-1}.

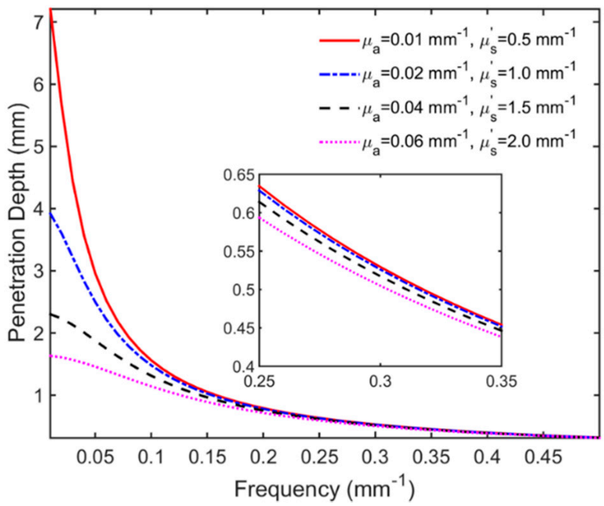

Figure 6. Relationship between light penetration depth and spatial frequency for a homogeneous sample under structured illumination of sinusoidal patterns with four sets of optical properties.

In order to improve estimation accuracy for optical properties of two-layered horticultural products by using the stepwise method, it is suggested to have relatively large spatial frequency for estimating μ_{a1} and $\mu_{s1}{}'$ through one-layered model, and relatively small frequency for estimating μ_{a2} and $\mu_{s2}{}'$ through two-variable fit based on two-layered model. Effect of tissue optical properties on frequency selection should also be taken into account, which is consistent with the suggestions discussed in Section 3.3 (i.e., optimize the spatial frequency in terms of $mfp_1{}'$ and/or $mfp_2{}'$).

4. Discussion

Depth-varying characterization is the hallmark of SFDI technique under structured illumination with sinusoidal patterns, which is absent in conventional uniform illumination. However, the light penetration depth derived from Equation (4) does not always hold for actually detectable region for a general imaging system. In such cases, the light backscattered close to the illumination source contributes more to the detected signals, which correspond to a far more superficial depth of tissue interrogation than that derived from diffuse light attenuation. Moreover, due to the comprehensive consideration of imaging resolution, imaging contrast and signal-to-noise ratio, the factor of $1/e$ for light decaying in tissues is not always appropriate in practical applications, such as the subsurface bruise detection of fruit sample [36]. Since one goal of this study is to explore the potential of accuracy improvement for estimating optical properties of two-layered horticultural products by selecting appropriate frequency region, the relationship between light penetration depth and spatial frequency was just roughly investigated here. A more realistic experimental setting, such as three-dimensional modeling of the target sample with more layers [37], should be taken into account in the future for quantifying the light penetration depth, as well as the sampling volume (i.e., spatial distribution of detector depth sensitivity).

The cross effect of each layer is one of the challenging factors influencing optical property estimation of two-layered horticultural products. It is desirable to obtain the effective information of the target (top or bottom) layer when estimating the corresponding μ_a and $\mu_s{}'$ without the interference of the other layer. The feature of depth-varying of SFDI provides a potential solution for solving this problem. The emitted optical signals under large spatial frequency carry more information related to the top layer, while those with relatively small spatial frequency penetrate deep into the bottom layer. It is thus possible to quantitatively select a spatial frequency, under which the captured signal is only related to the top layer. Then, an operation of subtraction between this signal and another one with smaller frequency can be used to eliminate the effect of the top layer. In principle, the signal after this operation should be more related to the bottom layer, and thus improving the estimation accuracy for μ_a and $\mu_s{}'$ of the bottom layer. Take the apple fruit as a two-layered example with peel and flesh tissues. Subtraction operation for the demodulated reflectance between the small frequency and large frequency is expected to clear the peel information of apple sample, and the remaining reflectance will be more valuable for estimating μ_a and $\mu_s{}'$ of the flesh tissue. It should be noted that this method may be limited for the two-layered horticultural products with relatively thin top-layer thickness (e.g., apple, peach and tomato) due to restricted light penetration depth (~1–2 mm) under the spatial frequency of 0.15 mm^{-1} [38]. The full potential of this method is worth exploring in the future research.

Thanks to the characteristics of the one-layered model, the stepwise method does not require a priori knowledge of the top-layer thickness for estimating μ_{a1} and $\mu_{s1}{}'$, but the top-layer thickness is still required to be known when estimating μ_{a2} and $\mu_{s2}{}'$ using the two-variable fit through the two-layered model. However, the top-layer thickness is usually unknown or difficult to be measured accurately, which brings challenges for optical property estimations of the bottom layer. Furthermore, the sample-based calibration method, which was employed for reflectance correction, may also bring some challenges when considering another optical property, i.e., the scattering phase function. Light backscattering at short source-detector separations is considerably influenced by the scattering phase function. In the spatial-frequency domain, as the horticultural product is illuminated by the structured lighting with high spatial frequency, part of the backscattered light would be referred to as sub-diffusive light, which largely depends on the scattering phase function. Different phase function parameters have been proposed for quantifying the influence of phase function on sub-diffusively backscattered light [39]. The influence of scattering phase function changed in the MC simulations on optical property estimations should be investigated.

In recent years, deep learning algorithms (e.g., generative adversarial networks, random forest, etc.) have evolved rapidly, which provide a means for accelerating and also improving optical property estimations of turbid materials [40–42]. What makes such methods attractive is their capacity to perform particularly well in learning nonlinear mappings. Unlike the conventional nonlinear curve fitting based on diffusion model, a deep learning method could predict optical properties directly from the SFDI images, without a priori knowledge of the top-layer properties (e.g., thickness, absorption and reduced scattering coefficients), which, however, require a sufficiently large image dataset to train the networks. Hence, future research efforts should also be directed at efficient utilization of deep learning for rapid and accurate optical property estimations of horticultural products.

5. Conclusions

This paper presents a theoretical analysis of intrinsic properties of the two-layered diffusion model and inverse algorithm through numerical simulation, including effect of optical parameter on reflectance prediction and optical property extraction, estimation accuracy of different curve fitting methods, and relationship between penetration depth and spatial frequency, in order to improve optical property estimation accuracy of two-layered horticultural products using SFDI technique. Reflectance prediction results indicated that there is good separation in diffuse reflectance over a large range of spatial frequencies for different $\mu_{s1}{}'$ values, whereas less separation in diffuse reflectance for different μ_{a1} values, and even less separation for different values of μ_{a2} and $\mu_{s2}{}'$, which is in agreement with accuracy for estimating optical properties. Evaluation of parameter estimation accuracy for all the five curve fitting strategies suggested to apply the stepwise method for estimating optical properties of two-layered samples, which estimated μ_{a1} and $\mu_{s1}{}'$ using the one-layered model first, followed with the estimation of μ_{a2} and μ_{s2}' using the two-variable fit. Investigation on the factors influencing the extraction of μ_{a1} and μ_{s1}', and relationship between penetration depth and spatial frequency offered great guidance for optimizing the frequency region for optical property estimation. Future work can be done on exploring the full potential of depth-varying features in SFDI for reducing or eliminating the effect of the top layer on estimating optical properties of the bottom layer.

Supplementary Materials: The following are available online at https://www.mdpi.com/2076-3417/11/2/617/s1, Figure S1: Absolute error contour maps for estimating μ_{a1} (left panel) and μ_{s1}' (right panel) of four representative two-layered simulation samples with varying values of μ_{a1}/μ_{a2} by using the stepwise method with different start and end frequencies, Figure S2: Absolute error contour maps for estimating μ_{a1} (left panel) and μ_{s1}' (right panel) of four representative two-layered simulation samples with varying values of μ_{s1}'/μ_{s2}' by using the stepwise method with different start and end frequencies, Table S1: Twenty two-layered simulation samples with different combinations of μ_{a1}, μ_{s1}', μ_{a2}, $\mu_{s2}'$and top-layer thickness d for investigating the effects of optical properties on reflectance prediction and comparing the estimation performance of diverse curve fitting methods, Table S2: Two-layered simulation samples with varying values of mfp_1'/mfp_2', Table S3: Two-layered simulation samples with varying values of μ_{a1}/μ_{a2}, Table S4: Two-layered simulation samples with varying values of μ_{s1}'/μ_{s2}', Table S5: Two-layered simulation samples with varying values of μ_{s1}'/μ_{a1}.

Author Contributions: Conceptualization, D.H. and Y.H.; methodology, D.H. and T.S.; software, D.H.; validation, Y.H. and Q.Z.; writing—original draft preparation, D.H.; writing—review and editing, D.H., Y.H., Q.Z. and T.S.; supervision, L.Y. and Z.Y.; funding acquisition, D.H. All authors have read and agreed to the published version of the manuscript.

Funding: This research was funded by the Natural Science Foundation of Zhejiang Province (LQ20C130002), the Natural and Science Foundation of China (32001414), the Project of Key Laboratory in the Ministry of Agriculture and Rural Areas (2016NYZD18003) and the Startup Project of Zhejiang A&F University (2034020090).

Acknowledgments: The authors gratefully thank Renfu Lu in the U.S. Department of Agriculture Agricultural Research Service (USDA/ARS) for his great guidance and valuable advice.

Conflicts of Interest: The authors declare no conflict of interest.

References

1. Huang, Y.; Lu, R.; Hu, D.; Chen, K. Quality assessment of tomato fruit by optical absorption and scattering properties. *Postharvest Biol. Technol.* **2018**, *143*, 78–85. [CrossRef]
2. Sun, C.; Van Beers, R.; Aernouts, B.; Saeys, W. Bulk optical properties of citrus tissues and the relationship with quality properties. *Postharvest Biol. Technol.* **2020**, *163*, 111127. [CrossRef]
3. Vanoli, M.; Van Beers, R.; Sadar, N.; Rizzolo, A.; Buccheri, M.; Grassi, M.; Lovati, F.; Nicolaï, B.; Aernouts, B.; Watté, R. Time-and spatially-resolved spectroscopy to determine the bulk optical properties of 'Braeburn'apples after ripening in shelf life. *Postharvest Biol. Technol.* **2020**, *168*, 111233. [CrossRef]
4. Kienle, A.; Patterson, M.S.; Dögnitz, N.; Bays, R.; Wagnières, G.; Van Den Bergh, H. Noninvasive determination of the optical properties of two-layered turbid media. *Appl. Opt.* **1998**, *37*, 779–791. [CrossRef] [PubMed]
5. Cen, H.; Lu, R. Quantification of the optical properties of two-layer turbid materials using a hyperspectral imaging-based spatially-resolved technique. *Appl. Opt.* **2009**, *48*, 5612–5623. [CrossRef]
6. Liemert, A.; Kienle, A. Analytical approach for solving the radiative transfer equation in two-dimensional layered media. *J. Quant. Spectrosc. Radiat. Transf.* **2012**, *113*, 559–564. [CrossRef]
7. Wang, A.; Wei, X. A sequential method for estimating the optical properties of two-layer agro-products from spatially-resolved diffuse reflectance: Simulation. *Artif. Intell. Agric.* **2019**, *3*, 69–78. [CrossRef]
8. Weber, J.R.; Cuccia, D.J.; Durkin, A.J.; Tromberg, B.J. Noncontact imaging of absorption and scattering in layered tissue using spatially modulated structured light. *J. Appl. Phys.* **2009**, *105*, 102028. [CrossRef]
9. Tabassum, S.; Pera, V.; Greening, G.; Muldoon, T.J.; Roblyer, D. Two-layer inverse model for improved longitudinal preclinical tumor imaging in the spatial frequency domain. *J. Biomed. Opt.* **2018**, *23*, 076011. [CrossRef]
10. Yudovsky, D.; Durkin, A.J. Spatial frequency domain spectroscopy of two layer media. *J. Biomed. Opt.* **2011**, *16*, 107005. [CrossRef]
11. Yudovsky, D.; Nguyen, J.Q.M.; Durkin, A.J. In Vivo spatial frequency domain spectroscopy of two layer media. *J. Biomed. Opt.* **2012**, *17*, 107006. [CrossRef] [PubMed]
12. Hu, D.; Lu, R.; Ying, Y. Spatial-frequency domain imaging coupled with frequency optimization for estimating optical properties of two-layered food and agricultural products. *J. Food Eng.* **2020**, *277*, 109909. [CrossRef]

13. Hu, D.; Lu, R.; Ying, Y.; Fu, X. A stepwise method for estimating optical properties of two-layer turbid media from spatial-frequency domain reflectance. *Opt. Express* **2019**, *27*, 1124–1141. [CrossRef]
14. Lu, Y.; Li, R.; Lu, R. Structured-illumination reflectance imaging (SIRI) for enhanced detection of fresh bruises in apples. *Postharvest Biol. Technol.* **2016**, *117*, 89–93. [CrossRef]
15. Hu, D.; Fu, X.; He, X.; Ying, Y. Noncontact and wide-field characterization of the absorption and scattering properties of apple fruit using spatial-frequency domain imaging. *Sci. Rep.* **2016**, *6*, 37920. [CrossRef] [PubMed]
16. Cuccia, D.J.; Bevilacqua, F.; Durkin, A.J.; Ayers, F.R.; Tromberg, B.J. Quantitation and mapping of tissue optical properties using modulated imaging. *J. Biomed. Opt.* **2009**, *14*, 024012. [CrossRef] [PubMed]
17. Svaasand, L.O.; Spott, T.; Fishkin, J.B.; Pham, T.; Tromberg, B.J.; Berns, M.W. Reflectance measurements of layered media with diffuse photon-density waves. *Phys. Med. Biol.* **1999**, *44*, 801–813. [CrossRef]
18. Hu, D.; Sun, T.; Yao, L.; Yang, Z.; Wang, A.; Ying, Y. Monte Carlo: A flexible and accurate technique for modeling light transport in food and agricultural products. *Trends Food Sci. Technol.* **2020**, *102*, 280–290. [CrossRef]
19. Wang, L.; Jacques, S.L.; Zheng, L. MCML-Monte carlo modeling of photon transport in multi-layered tissues. *Comput. Methods Programs Biomed.* **1995**, *47*, 131–146. [CrossRef]
20. Lu, R.; Van Beers, R.; Saeys, W.; Li, C.; Cen, H. Measurement of optical properties of fruits and vegetables: A review. *Postharvest Biol. Technol.* **2020**, *159*, 111003. [CrossRef]
21. Xie, D.; Guo, W. Measurement and Calculation Methods on Absorption and Scattering Properties of Turbid Food in Vis/NIR Range. *Food Bioprocess Technol.* **2020**, *13*, 229–244. [CrossRef]
22. Henyey, L.G.; Greenstein, J.L. Diffuse radiation in the galaxy. *Astrophys. J.* **1941**, *93*, 70–83. [CrossRef]
23. Saeys, W.; Velazco-Roa, M.A.; Thennadil, S.N.; Ramon, H.; Nicolai, B.M. Optical propertie of apple skin and flesh in the wavelength range from 350 to 2200 nm. *Appl. Opt.* **2008**, *47*, 908–919. [CrossRef] [PubMed]
24. Zhang, M.; Li, C.; Yang, F. Optical properties of blueberry flesh and skin and Monte Carlo multi-layered simulation of light interaction with fruit tissues. *Postharvest Biol. Technol.* **2019**, *150*, 28–41. [CrossRef]
25. Sun, C.; Aernouts, B.; Van Beers, R.; Saeys, W. Simulation of light propagation in citrus fruit using monte carlo multi-layered (MCML) method. *J. Food Eng.* **2021**, *291*, 110225. [CrossRef]
26. Aster, R.C.; Borchers, B.; Thurber, C.H. *Parameter Estimation and Inverse Problems*; Academic Press: Cambridge, MA, USA, 2011; Volume 90.
27. Hu, D.; Lu, R.; Ying, Y. Finite element simulation of light transfer in turbid media under structured illumination. *Appl. Opt.* **2017**, *56*, 6035–6042. [CrossRef]
28. Gigan, S. Optical microscopy aims deep. *Nat. Photonics* **2017**, *11*, 14–16. [CrossRef]
29. Fraser, D.G.; Jordan, R.B.; Kunnemeyer, R.; McGlone, V.A. Light distribution inside mandarin fruit during internal quality assessment by NIR spectroscopy. *Postharvest Biol. Technol.* **2003**, *27*, 185–196. [CrossRef]
30. Qin, J.; Lu, R. Monte Carlo simulation for quantification of light transport features in apples. *Comput. Electron. Agric.* **2009**, *68*, 44–51. [CrossRef]
31. Wang, W.; Li, C. Measurement of the light absorption and scattering properties of onion skin and flesh at 633 nm. *Postharvest Biol. Technol.* **2013**, *86*, 494–501. [CrossRef]
32. Chugunov, S.; Li, C. Monte Carlo simulation of light propagation in healthy and diseased onion bulbs with multiple layers. *Comput. Electron. Agric.* **2015**, *117*, 91–101. [CrossRef]
33. Askoura, M.L.; Vaudelle, F.; L'Huillier, J.-P. Numerical study of light transport in apple models based on Monte Carlo simulations. *Photonics* **2016**, *3*, 2. [CrossRef]
34. Tromberg, B.J.; Svaasand, L.O.; Tsay, T.-T.; Haskell, R.C. Properties of photon density waves in multiple-scattering media. *Appl. Opt.* **1993**, *32*, 607–616. [CrossRef] [PubMed]
35. Cuccia, D.J.; Bevilacqua, F.; Durkin, A.J.; Tromberg, B.J. Modulated imaging quantitative analysis and tomography of turbid media in the spatial-frequency domain. *Opt. Lett.* **2005**, *30*, 1354–1356. [CrossRef]
36. Lu, Y.; Li, R.; Lu, R. Gram-Schmidt orthonormalization for retrieval of amplitude images under sinusoidal patterns of illumination. *Appl. Opt.* **2016**, *55*, 6866–6873. [CrossRef]
37. Meglinsky, I.; Matcher, S. Modelling the sampling volume for skin blood oxygenation measurements. *Med. Biol. Eng. Comput.* **2001**, *39*, 44–50. [CrossRef]
38. Hayakawa, C.K.; Karrobi, K.; Pera, V.E.; Roblyer, D.M.; Venugopalan, V. Optical sampling depth in the spatial frequency domain. *J. Biomed. Opt.* **2018**, *24*, 071603. [CrossRef]
39. Bodenschatz, N.; Krauter, P.; Liemert, A.; Kienle, A. Quantifying phase function influence in subdiffusively backscattered light. *J. Biomed. Opt.* **2016**, *21*, 035002. [CrossRef]
40. Panigrahi, S.; Gioux, S. Machine learning approach for rapid and accurate estimation of optical properties using spatial frequency domain imaging. *J. Biomed. Opt.* **2018**, *24*, 071606. [CrossRef]
41. Zhao, Y.; Deng, Y.; Bao, F.; Peterson, H.; Istfan, R.; Roblyer, D. Deep learning model for ultrafast multifrequency optical property extractions for spatial frequency domain imaging. *Opt. Lett.* **2018**, *43*, 5669–5672. [CrossRef]
42. Chen, M.T.; Mahmood, F.; Sweer, J.A.; Durr, N.J. GANPOP: Generative Adversarial Network Prediction of Optical Properties from Single Snapshot Wide-field Images. *IEEE Trans. Med. Imaging* **2019**, *39*, 1988–1999. [CrossRef] [PubMed]